Acta Mech. Sin.
DOI 10.1007/s10409-017-0657-8

RESEARCH PAPER

Optomechanical soft metamaterials

Xiangjun Peng[1,2] · **Wei He**[1,2] · **Yifan Liu**[1,2] · **Fengxian Xin**[1,2] · **Tian Jian Lu**[1,2]

Received: 20 February 2017 / Accepted: 2 March 2017

Abstract We present a new type of optomechanical soft metamaterials, which is different from conventional mechanical metamaterials, in that they are simple isotropic and homogenous materials without resorting to any complex nano/microstructures. This metamaterial is unique in the sense that its responses to uniaxial forcing can be tailored by programmed laser inputs to manifest different nonlinear constitutive behaviors, such as monotonic, S-shape, plateau, and non-monotonic snapping performance. To demonstrate the novel metamaterial, a thin sheet of soft material impinged by two counterpropagating lasers along its thickness direction and stretched by an in-plane tensile mechanical force is considered. A theoretical model is formulated to characterize the resulting optomechanical behavior of the thin sheet by combining the nonlinear elasticity theory of soft materials and the optical radiation stress theory. The optical radiation stresses predicted by the proposed model are validated by simulations based on the method of finite elements. Programmed optomechanical behaviors are subsequently explored using the validated model under different initial sheet thicknesses and different optical inputs, and the first- and second-order tangential stiffness of the metamaterial are used to plot the phase diagram of its nonlinear constitutive behaviors. The proposed optomechanical soft metamaterial shows great potential in biological medicine, microfluidic manipulation, and other fields.

Keywords Optomechanics · Soft metamaterial · Optical radiation stress · Programmable constitutive relation

1 Introduction

Metamaterials typically refer to artificial materials with purposely designed internal structures that enable unusual physical behaviors [1] and hence a wide range of innovative designing. Such materials are commonly constructed with novel geometries to realize their special properties. For electromagnetic properties, Smith et al. [2] first demonstrated a composite medium with negative permittivity and permeability both by simulation and experiment, opening a new avenue for transformation optics. The study by Pendry [3] designed subwavelength lenses using negative refractive index materials. In their work, Schurig et al. [4] described the first practical realization of electromagnetic cloak with the use of optical metamaterials.

While significant advances in optical metamaterials for constructing novel optic devices have been reported, such concepts also inspire research on mechanical metamaterials. Mechanical metamaterials, typically characterized by negative constants, possess fantastic properties such as negative compressibility transitions [5], negative incremental stiffness [6,7], negative normal stress [8], as well as negative Poisson's ratio [9–12]. More recently, a new type of mechanical metamaterial was found by harnessing instabilities with a wide variety of potential applications has been proposed. The study by Li et al. [13] exploited the elastic instability of shape mem-

✉ Fengxian Xin
fengxian.xin@gmail.com

Tian Jian Lu
tjlu@mail.xjtu.edu.cn

[1] State Key Laboratory for Strength and Vibration of Mechanical Structures, Xi'an Jiaotong University, Xi'an 710049, China

[2] MOE Key Laboratory for Multifunctional Materials and Structures, Xi'an Jiaotong University, Xi'an 710049, China

Published online: 23 March 2017

ory polymer sheets with an array of holes and demonstrated color switching due to pattern transformations. In their work, Overvelde et al. [14] designed and fabricated fluidic actuators by harnessing snap-through instabilities, which can generate high forces and fast actuation. Their study provided a new methodology for designing soft actuators having small volume. Further, Singamaneni et al. [15] demonstrated that buckling instability can be harnessed in porous elasto-plastic solids to obtain a dramatic pattern transformation, which can be used to design tunable photonic crystals or scaffolds for tissue engineering. A paper by Shan et al. [16] proposed a new class of mechanical metamaterials, containing beam elements specially designed to enable local bistable deformation to trap energy. Nonetheless, to accomplish a special purpose, most existing mechanical metamaterials are either designed with complicated structures or embedded with foreign inclusions to gain special properties, which significantly increases difficulties in fabrication. There is thus a pressing need to design metamaterials that can be fabricated from an isotropic and homogenous medium such as soft material.

In this study, we create an optomechanical soft metamaterial with programmable mechanical constitutive relation via electromagnetic inputs. We propose a theoretical model to investigate the optomechanical response of this soft metamaterial and, upon tuning the electromagnetic wave inputs, reveal phase transition of such metamaterial. This study provides a new yet simple method for fabricating optomechanical devices with small features and switchable properties.

2 Theoretical model

An electromagnetic wave carries momentum flux when it propagates through a medium from a surrounding medium, generating optical force on the illuminated surface, which is quite like the acoustic radiation force [17,18]. Such force can be expressed in the form of a stress tensor, called the Maxwell stress, which is associated with the electromagnetic field in each medium and can be written as [19]

$$\boldsymbol{T} = (\varepsilon \boldsymbol{E} \otimes \boldsymbol{E} + \mu \boldsymbol{H} \otimes \boldsymbol{H}) - \frac{1}{2}(\varepsilon \boldsymbol{E} \cdot \boldsymbol{E} + \mu \boldsymbol{H} \cdot \boldsymbol{H})\boldsymbol{I}, \quad (1)$$

where $\boldsymbol{E}$ is the electric field, H is the magnetic field, I is the identity matrix, ε is the permittivity, and μ is the permeability.

Although the optical force is feeble, the force becomes stronger when it comes to lasers. Equation (1) indicates that the Maxwell stress scales with εE^2 and μH^2 . Since lasers are harmonic plane waves, the two components of the electromagnetic fields (i.e., electric field and magnetic field) are governed by $\varepsilon E^2 = \mu H^2 = \sqrt{\varepsilon\mu} EH$ [20]. Knowing that $c = 1/\sqrt{\varepsilon\mu}$ is the speed of light and EH is equal to the flux of energy, we obtain that the magnitude of Maxwell stress scales as $P/(cA)$, P being the input power and A the cross-sectional area of a beam of light. For typical values of lasers such as $P = 0.1$ W, $A = 1\ \mu\text{m}^2$, and $c = 3 \times 10^8$ m/s, we find the magnitude of Maxwell stress is about 300 Pa. Soft materials such as gels can have elastic moduli as low as 100 Pa [21,22]. As a result, theoretically speaking, Maxwell stresses generated by lasers can induce large deformation in soft materials. Indeed, previous experiments confirmed large laser-induced optical forces, which can be used to manipulate solid particles [23–26], stretch cells [27,28], deform fluid interfaces [29–31], and bend solid waveguides [32–37]. Further, reversible phase transition in polymer gel was induced by optical forces induced by lasers [38]. Therefore, laser-induced optical forces can be harnessed to generate large deformation in soft materials with attractive non-contact and fast manipulation properties.

Intrinsically, the Maxwell stress determines the deformation of a soft material through its time-average over an oscillation circle of an electromagnetic wave, as

$$\langle \boldsymbol{T} \rangle = \frac{1}{2}\text{Re}\left[\left(\varepsilon \boldsymbol{E} \otimes \boldsymbol{E}^* + \mu \boldsymbol{H} \otimes \boldsymbol{H}^*\right) - \frac{1}{2}\left(\varepsilon \boldsymbol{E} \cdot \boldsymbol{E}^* + \mu \boldsymbol{H} \cdot \boldsymbol{H}^*\right)\boldsymbol{I} \right], \quad (2)$$

where the superscript "*" represents the complex-conjugate of the corresponding variable.

To give an intuitive sense of the optical force due to lasers, we plot in Fig. 1 the distribution of time-averaged Maxwell stress in both the soft material sheet and the surrounding medium. The sheet optically mismatches with the surrounding medium, causing transmission and reflection of lasers at the interfaces. The stress in the sheet differs from that outside, and it is such difference at material interface induces a nonzero equivalent stress to deform the soft sheet.

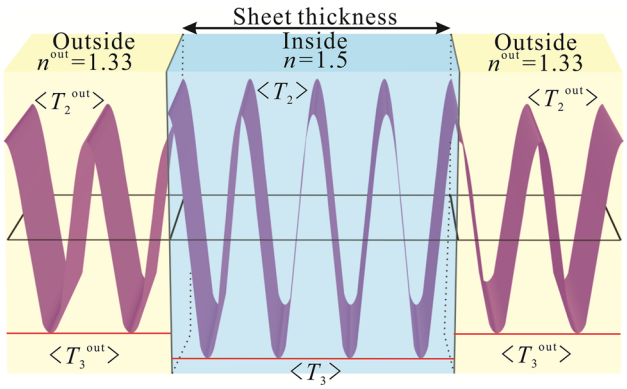

Fig. 1 Distribution of time-averaged Maxwell stress in soft material sheet (refractive index $n = 1.5$) and its surrounding medium ($n^{\text{out}} = 1.33$)

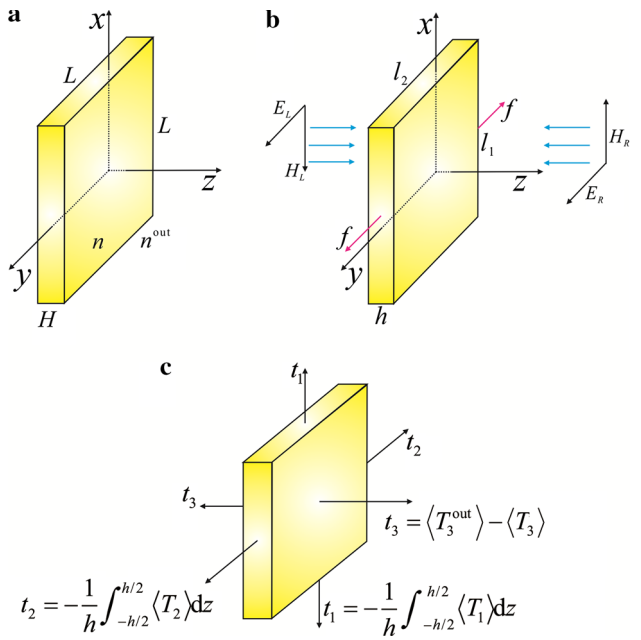

Fig. 2 Tensional mechanical force and two antiparallel lasers deform a thin sheet of soft metamaterial with refractive index (n) different from that in surrounding medium (n^{out}). **a** The sheet has dimensions (L, L, H) in reference state. **b** Two counterpropagating lasers impinge the sheet in the z-direction while a tensional mechanical force f loads the sheet in the y-direction. Under combined optical and mechanical forces, the sheet deforms to current dimensions (l_1, l_2, h). **c** Equivalent mechanical stresses in the sheet induced by Maxwell stress and tensional mechanical force

We assume the soft material is homogenous and isotropic, without free charge or current in it. Moreover, the soft material is considered to be an ideal material with constant permittivity and permeability when undergoing mechanical deformation. Note that, when excited by lasers with high enough frequencies (e.g., $\geqslant 10^{14}$ Hz, far exceeding the mechanical frequencies), the soft material cannot respond to such fast electromagnetic oscillation as a result of material hysteresis. Thus, we can regard the stress generated by lasers as a steady-state time-averaged stress, which can cause steady material deformation.

With reference to Fig. 2a, consider a thin sheet of soft material sheet with initial dimensions (L, L, H) and refractive index n immersed in an isotropic medium with refractive index n^{out}. Cartesian coordinates (x, y, z) located on sheet midplane ($z = 0$) are selected. As shown in Fig. 2b, when the sheet is loaded by a tensional mechanical force f in the y-direction and impinged by two antiparallel lasers having identical phase position, frequency, and amplitude, but opposite propagation directions, the sheet is deformed from its reference state of Fig. 2a to current dimensions (l_1, l_2, h). Let $E_L = E_0 \exp(-\mathrm{i}k^{\text{out}}z)$ and $H_L = \sqrt{\varepsilon^{\text{out}}/\mu}E_0 \exp(-\mathrm{i}k^{\text{out}}z)$ be the left side fields, where E_0 is the amplitude of the electric field, $\varepsilon^{\text{out}} = (n^{\text{out}})^2\varepsilon_0$ is the permittivity of the surrounding medium, μ is the permeability of both the soft material and the surrounding medium, $k^{\text{out}} = n^{\text{out}}\omega/c_0$ is the wave number of the lasers, ω is the angular frequency, and c_0 is the speed of light in vacuum. Because of the symmetry of the setup, the right side fields are not listed. As the two fields of lasers are symmetric with the respect to sheet midplane, the lasers generate optical forces that have opposite directions and identical magnitude, maintaining the midplane stationery. This process is closely linked to the Maxwell stress tensor $\boldsymbol{T}$ at the interface, generating equivalent principal stresses (Fig. 2c) as

$$t_1 = -\frac{1}{h}\int_{-h/2}^{h/2} \langle T_1(z)\rangle \mathrm{d}z, \tag{3}$$

$$t_2 = -\frac{1}{h}\int_{-h/2}^{h/2} \langle T_2(z)\rangle \mathrm{d}z, \tag{4}$$

$$t_3 = \left\langle T_3^{\text{out}}(h)\right\rangle - \langle T_3(h)\rangle, \tag{5}$$

where ($\langle T_1\rangle, \langle T_2\rangle$, and $\langle T_3\rangle$) are the principal Maxwell stresses obtained by time-averaging $\boldsymbol{T}$ over a period of electromagnetic oscillation, i.e., $\langle \boldsymbol{T}\rangle = (\omega/2\pi)\int_0^{2\pi/\omega} \boldsymbol{T}\mathrm{d}t$. Here, the components of the electric and magnetic field are taken as ($E_1 = E_0, E_2 = E_3 = 0$) and ($H_2 = H_0, H_1 = H_3 = 0$), respectively. Under such conditions, Eq. (2) indicates that only the principal Maxwell stresses are nonzero

$$\langle T_1\rangle = -\langle T_2\rangle = \frac{1}{4}\left(\varepsilon|E_{\text{a}}|^2 - \mu|H_{\text{a}}|^2\right), \tag{6}$$

$$\langle T_3\rangle = -\frac{1}{4}\left(\varepsilon|E_{\text{a}}|^2 + \mu|H_{\text{a}}|^2\right), \tag{7}$$

where E_{a} and H_{a} are the electric field and magnetic field in medium "a". Detailed expressions of the electromagnetic field for the considered case are presented in "Appendix".

Like many existing studies on nonlinear deformation of soft materials, we consider only homogenous deformation of principal stretches $\lambda_1 = l_1/L, \lambda_2 = l_2/L, \lambda_3 = h/H$. The two components (electric field and magnetic field) of the electromagnetic field are determined by wave propagation of the two lasers, depending on key parameters such as the refractive indexes of soft material and outside medium, laser wavelength in soft material, and sheet thickness. Consequently, the equivalent principal stresses derived on the basis of electromagnetic field are also dependent upon these parameters. In Fig. 3, we plot the normalized equivalent stresses $t_i/(\varepsilon_0 E_0^2)$ as functions of in-plane stretch λ_2 for fixed optical input of $\varepsilon_0 E_0^2/G = 1$ but different initial sheet thicknesses: **a** $H/\Lambda = 0.5$, **b** $H/\Lambda = 1.5$, **c** $H/\Lambda = 3.5$, and **d** $H/\Lambda = 4.5$, where $\Lambda = 2\pi c_0/\omega$ is laser wavelength in the soft material. For validation, numerical results obtained using finite-element package COMSOL Multiphysics are compared with the present theoretical predictions. Excellent agreement between theory and simulation is achieved, as

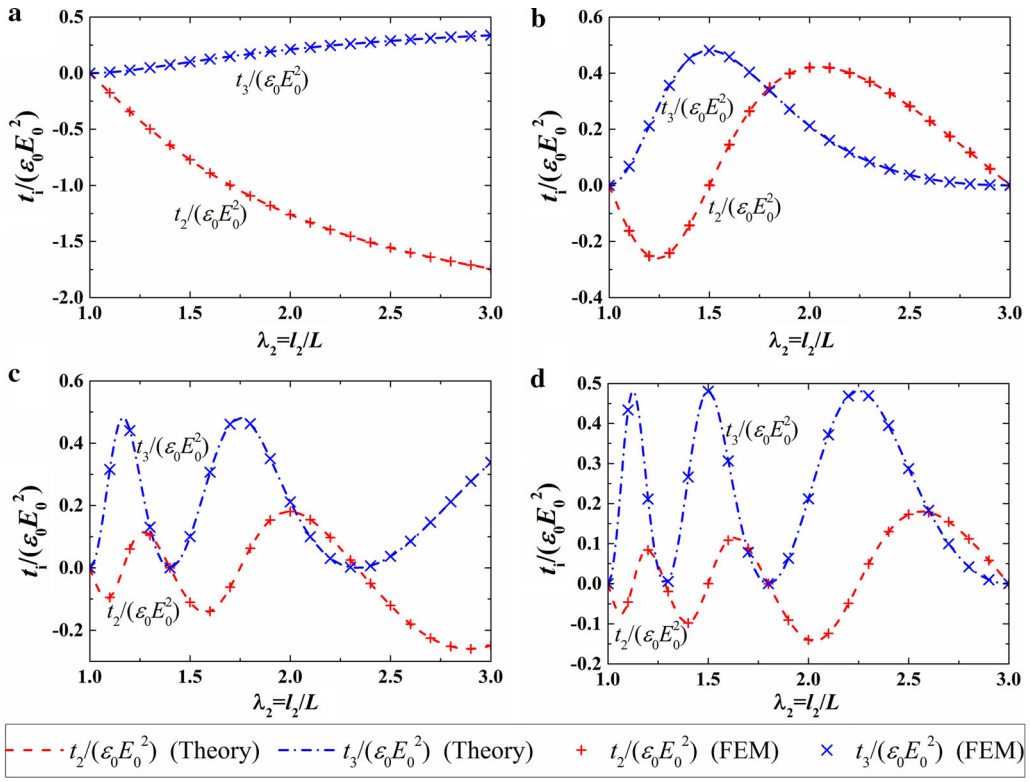

Fig. 3 Theoretical predictions compared with numerical simulation results of normalized equivalent stresses for fixed optical input ($\varepsilon_0 E_0^2/G = 1$) but different initial sheet thicknesses: **a** $H/\Lambda = 0.5$, **b** $H/\Lambda = 1.5$, **c** $H/\Lambda = 3.5$, and **d** $H/\Lambda = 4.5$

shown in Fig. 3. As H/Λ is increased, it is seen that the stress versus stretch curves become considerably more undulating.

To analyze the instability behavior of the soft sheet, we constrain its length in the x-direction. When it comes to large deformation, the change in shape of the soft material is much larger than its volume change. Thus, we further assume that the soft material is incompressible so that its principal stretches can be rewritten as $\lambda_1 = 1$ and $\lambda_3 = 1/\lambda_2$. Under such conditions, capturing the fundamental physical nature of the optomechanical soft material becomes relatively straightforward, as demonstrated below.

Combining the electrodynamics of light and the nonlinear elasticity theory of soft materials, we establish an optomechanical model for the proposed soft metamaterial. To this end, we represent its elasticity by employing the Gent model [39], as

$$W(\boldsymbol{F}) = -\frac{G J_{\lim}}{2} \ln\left(1 - \frac{\lambda_1^2 + \lambda_2^2 + \lambda_3^2 - 3}{J_{\lim}}\right), \tag{8}$$

where G and $J_{\lim}$ are the shear modulus and extension limit of the soft material, and $\boldsymbol{F}$ is the deformation gradient. Correspondingly, the Cauchy stress is expressed as [40]

$$\boldsymbol{\sigma} = \boldsymbol{F}\frac{\partial W(\boldsymbol{F})}{\partial \boldsymbol{F}} + \boldsymbol{t} - \Pi \boldsymbol{I}, \tag{9}$$

where Π is the Lagrange multiplier introduced to satisfy the constraint of material incompressibility. Since the soft material is considered incompressible, the above equation can be rewritten as

$$\sigma_1 - \sigma_3 = \lambda_1 \frac{\partial W(\lambda_1, \lambda_2)}{\partial \lambda_1} + \langle T_1 \rangle - \langle T_3 \rangle, \tag{10}$$

$$\sigma_2 - \sigma_3 = \lambda_2 \frac{\partial W(\lambda_1, \lambda_2)}{\partial \lambda_2} + \langle T_2 \rangle - \langle T_3 \rangle. \tag{11}$$

In the y-direction, $\sigma_2 = f/(l_1 h)$. Incorporating the boundary problem conditions to Eq. (7), we get

$$t_2 - t_3 + \frac{f}{l_1 h} = \frac{G\left(\lambda_2^2 - \lambda_3^2\right)}{1 - \left(\lambda_1^2 + \lambda_2^2 + \lambda_3^2 - 3\right)/J_{\lim}}. \tag{12}$$

Such equation can be rewritten as

$$\tilde{F} = \left[-\frac{t_2(\lambda_2) - t_3(\lambda_2)}{G} + \frac{\left(\lambda_2^2 - \lambda_2^{-2}\right)}{1 - \left(1 + \lambda_2^2 + \lambda_2^{-2} - 3\right)/J_{\lim}}\right]\lambda_2^{-1}, \tag{13}$$

where $\tilde{F} = f/(GLH)$ is the normalized tensional mechanical force, which is a function of stretch λ_2, electric field amplitude E_0 (or magnetic field amplitude H_0) and initial sheet thickness H.

Equation (13) determines the normalized force $\tilde{F}$ versus stretch λ_2 relation. To analyze further the optomechanical response of the metamaterial, we use the first- and second-order tangential stiffness of Eq. (13) to separate its responses under different modes, as

$$\frac{\partial \tilde{F}}{\partial \lambda_2} = \frac{\partial \tilde{F}}{\partial \lambda_2}\left(\frac{\varepsilon_0 E_0^2}{G}, \frac{H}{\Lambda}, \lambda_2\right) = 0, \tag{14}$$

$$\frac{\partial^2 \tilde{F}}{\partial \lambda_2^2} = \frac{\partial^2 \tilde{F}}{\partial \lambda_2^2}\left(\frac{\varepsilon_0 E_0^2}{G}, \frac{H}{\Lambda}, \lambda_2\right) = 0. \tag{15}$$

The stability of the current optomechanical system is determined by Eqs. (14) and (15) by ensuring stretch λ_2 has real solution within the formulary parameter space of $\left(\varepsilon_0 E_0^2/G, H/\Lambda\right)$. As illustrated in the following section, Eq. (14) separates the S-shape region from the snapping region while Eq. (15) distinguishes the S-shaped region from the monotonic region.

3 Results and discussion

Figure 4a–d plots the normalized force as a function of in-plane stretch λ_2 for selected initial sheet thicknesses. Also plotted in each force–stretch diagram is the corresponding normalized equivalent stresses generated by lasers. For plotting, the amplitude of input optical field is fixed at $\varepsilon_0 E_0^2/G = 1$ while the normalized initial sheet thickness is varied as $H/\Lambda = 0.5, 1.5, 3.5, 4.5$. As H/Λ is increased, the force versus stretch curve exhibits four distinct variation tendencies. (1) Monotonic morphology of Fig. 4a in which the normalized force–stretch curve increases monotonically, accompanied by a negative second-order tangential stiffness, and nonlinear soft material deformation dominates the variation tendency. (2) S-shape of Fig. 4b in which the curve increases as well, but with a positive second-order tangential stiffness when the inflexion part emerges. In this case, the normalized equivalent stress–stretch curve becomes non-monotonic and $(t_2 - t_3)/\left(\varepsilon_0 E_0^2\right)$ plays a minor role in creating the inflexion. Fig. 4a, b shows that the soft material deforms in a succession of states of equilibrium. (3) Snapping shape of Fig. 4c where the curve goes up, down, and then up again. The sheet is prone to snapping-through instability, in which the tensional mechanical force is programmed to increase slowly. When the force attains local maximum, no state of equilibrium exists as the force goes up further; instead, the sheet snaps to a state of equilibrium with a larger stretch. In this case, the snapping-through

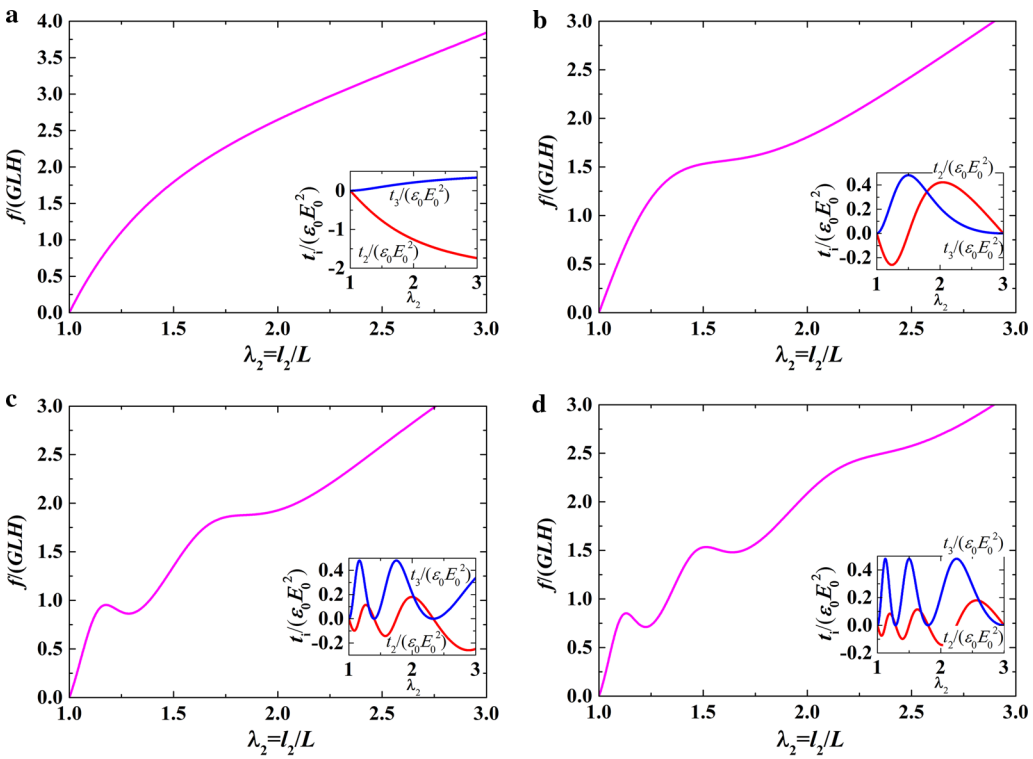

Fig. 4 Normalized mechanical force plotted as a function of stretch for optomechanical metamaterial sheet with fixed optical input $\varepsilon_0 E_0^2/G = 1$ at different initial sheet thicknesses: **a** $H/\Lambda = 0.5$, **b** $H/\Lambda = 1.5$, **c** $H/\Lambda = 3.5$, and **d** $H/\Lambda = 4.5$. As H/Λ is increased, the force–stretch curve sequentially exhibits monotonic, S-shape, snapping, and multi-snapping morphologies. *Inset plots* illustrate the variation trends of normalized optical stresses with stretch

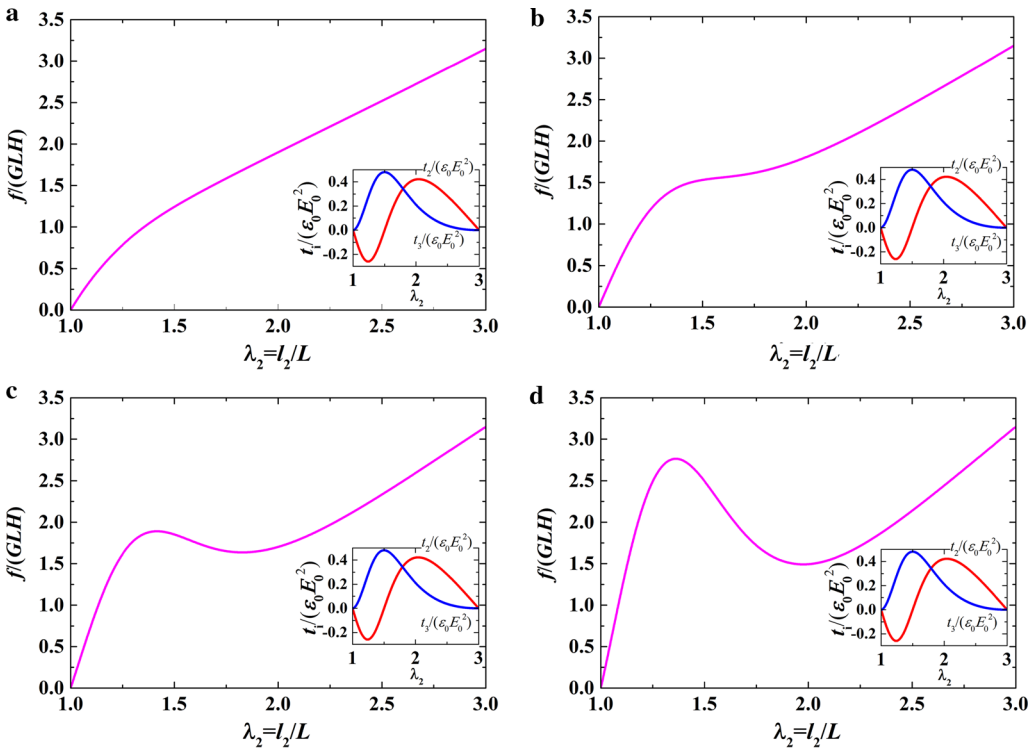

Fig. 5 Normalized mechanical force plotted as a function of stretch for optomechanical metamaterial sheet with a fixed initial sheet thickness of $H/\Lambda = 1.5$ at different optical inputs: **a** $\varepsilon_0 E_0^2/G = 0.2$, **b** $\varepsilon_0 E_0^2/G = 1$, **c** $\varepsilon_0 E_0^2/G = 2$, and **d** $\varepsilon_0 E_0^2/G = 4$. With increasing input optical field, the force–stretch curve sequentially exhibits monotonic, S-shape, snapping, and deep-snapping morphologies. *Inset plots* illustrate the variation trends of normalized optical stresses with stretch

instability occurs because the first-order tangential stiffness becomes negative and the equivalent stresses exerts a much larger influence on snapping. (4) Multi-snapping shape of Fig. 4d in which the curve varies non-monotonically and exhibits multiple snapping-through instabilities, caused by the multiple approaching of $t_2/\left(\varepsilon_0 E_0^2\right)$ and $t_3/\left(\varepsilon_0 E_0^2\right)$.

Next, consider the actuation of a sheet with fixed initial thickness of $H/\Lambda = 1.5$, but varying amplitude of optical field as $\varepsilon_0 E_0^2/G = 0.2$, 1, 2, 4. The normalized force versus stretch curves are presented in Fig. 5, with the corresponding normalized mechanical equivalent stresses caused by lasers included as insets in each diagram. Since the equivalent stresses depend on H/Λ, their variation tendency remains unchanged as the optical field changes its amplitude. However, the force versus stretch curves are significantly influenced as $\varepsilon_0 E_0^2/G$ is changed. With increasing optic wave input, these curves exhibit four distinct morphologies: monotonic, S-shape, snapping, and deep snapping. That is to say, large input optical fields tend to cause snapping-through instability. In this regime, the soft material deforms discontinuously. In sharp contrast, relatively small inputs ensure the sheet deforms in a succession of equilibrium states. The reason for such difference, as can be seen from Eq. (13), is that a larger input optical field enhances the effect of λ_2^{-1} while a smaller one weakens such effect.

Borrowing the concept of phase transition of three different phases in thermodynamics, we solve Eqs. (14) and (15) by ensuring the in-plane stretch λ_2 has real solution within the parameter space of $\left(\varepsilon_0 E_0^2/G, H/\Lambda\right)$. Different deformation states, as well as phase diagrams of optomechanical responses are thence obtained, for both optically mismatched $\left(n \neq n^{\text{out}}\right)$ and optically matched $\left(n = n^{\text{out}}\right)$ cases. Equation (14) distinguishes the positive first-order tangential stiffness from the negative one while Eq. (15) divides the positive and negative second-order tangential stiffnesses. Thus, Eqs. (14) and (15) divide the diagram into three phases, representing different optomechanical responses: (1) monotonic region, (2) S-shape region, and (3) snapping region, with an illustrative example given as inset in each category.

As can be seen from the phase diagram presented in Fig. 6, for a soft sheet with small initial thickness and low input optical field, its force–stretch curve tends to exhibit monotonic shape, while for a sheet with either larger initial thickness or input optical field, the S-shape and even snapping are readily achieved. The S-shape curve has a positive first-order tangential stiffness during actuation, while the snapping curve has a negative first-order tangential stiffness when snapping-through instability occurs. Between the S-shape and snapping regimes is a boundary line, of which the first tangential stiffness is zero before it becomes positive again (related to

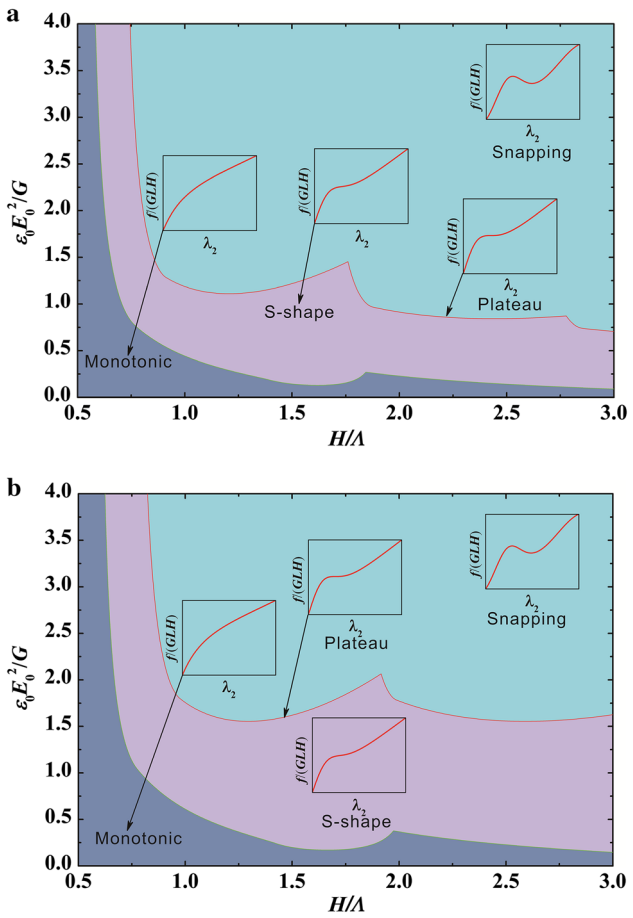

Fig. 6 Optomechanical phase diagrams for a thin soft metamaterial sheet subject to a combined uniaxial mechanical force and optical force in the parameter space $\left(\varepsilon_0 E_0^2/G, H/\Lambda\right)$, showing different nonlinear constitutive behaviors for both **a** optical mismatch case $n \neq n^{\text{out}}$ and **b** optical match case $n = n^{\text{out}}$

plateau response). Helped by these phase diagrams, we can predict the optomechanical response of the thin soft sheet once its initial thickness and the amplitude of input optical field are known.

4 Conclusions

We have presented a new class of optomechanical soft metamaterials that exhibit different kinds of mechanical responses by tailoring electromagnetic wave inputs. Under programmed lasers, this novel metamaterial, which is homogenous and isotropic, possesses unusual mechanical properties without resorting to embedded foreign inclusions or complicated artificial architectures. Further, the optical field can be easily modulated due to its fast and non-contact properties. Thus, our work creates an enormous space for innovation in conceptual design and fabrication of optomechanical devices that are promising for a wide range of potential applications, including using light to control light, fabricating optical circuits reconfigurable by optical forces, microfluidic manipulation platforms, etc.

Acknowledgements This work was supported by the National Natural Science Foundation of China (Grant 51528501) and the Fundamental Research Funds for Central Universities (Grant 2014qngz12).

Appendix: Electromagnetic wave propagation

With reference to Fig. 2, we consider an electromagnetic wave with electric component $E(z) = E_0 \exp\left(-\mathrm{i}k^{\text{out}}z\right)$ and magnetic component $H(z) = H_0 \exp\left(-\mathrm{i}k^{\text{out}}z\right)$ that impinges on a thin soft material sheet from its surrounding medium, where $H_0 = E_0/\eta$ and $\eta = \sqrt{\mu/\varepsilon}$ is the characteristic impedance of the medium. The soft material is considered to be an ideal material with constant permittivity and permeability when undergoing mechanical deformation. The propagation of electromagnetic wave in a source-free medium is governed by the Maxwell equations: $\nabla \times \boldsymbol{E} = -\partial \boldsymbol{B}/\partial t, \nabla \times \boldsymbol{H} = \partial \boldsymbol{D}/\partial t, \nabla \cdot \boldsymbol{D} = 0, \nabla \cdot \boldsymbol{B} = 0, \boldsymbol{E}$ the electric field, $\boldsymbol{H}$ the magnetic field, $\boldsymbol{D} = \varepsilon \boldsymbol{E}$ the electric flux density, and $\boldsymbol{B} = \mu \boldsymbol{H}$ the magnetic flux density. ε is the permittivity and μ is the permeability of the medium. Since the magnetic field corresponds to the electric field, the propagation of electromagnetic wave can be illustrated by the propagation of electric wave as shown in Fig. A1.

At the interface between the soft material sheet and the surrounding medium, the electromagnetic wave must satisfy the continuity conditions. Next consider the first interface of Fig. A1. The corresponding continuity conditions are $\boldsymbol{n} \times (\boldsymbol{E}_2 - \boldsymbol{E}_1) = 0, \boldsymbol{n} \times (\boldsymbol{H}_2 - \boldsymbol{H}_1) = 0$, where $\boldsymbol{n}$ is the

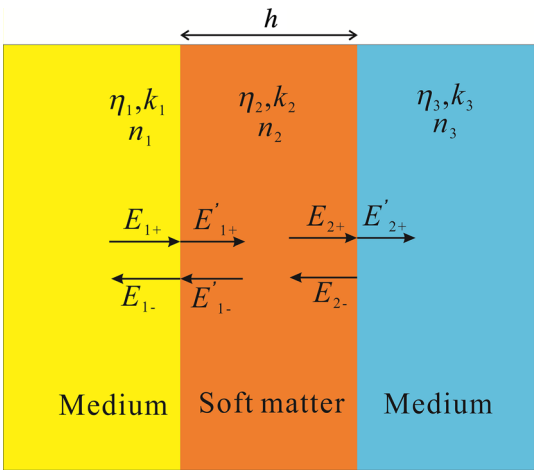

Fig. A1 Electric wave propagation through a soft material sheet as a representative of electromagnetic wave propagation. Subscripts "+" and "−" are related to positive- and negative-going waves, and superscript "′ " implies the right side of the interface

unit vector normal to the interface and the subscripts 1 and 2 indicate the left side and the right side of the interface, respectively. At the first interface we have

$$\begin{aligned} &E_{1+}+E_{1-}=E'_{1+}+E'_{1-},\\ &\frac{1}{\eta_1}\left(E_{1+}-E_{1-}\right)=\frac{1}{\eta_2}\left(E'_{1+}-E'_{1-}\right), \end{aligned} \tag{A1}$$

which can be written in matrix form as

$$\begin{bmatrix} E_{1+}\\ E_{1-}\end{bmatrix}=\frac{1}{\tau_1}\begin{bmatrix} 1 & \rho_1\\ \rho_1 & 1\end{bmatrix}\begin{bmatrix} E'_{1+}\\ E'_{1-}\end{bmatrix}, \tag{A2}$$

where $\rho_1=(\eta_2-\eta_1)/(\eta_1+\eta_2)$ and $\tau_1=2\eta_2/(\eta_1+\eta_2)$ are the elementary reflection and transmission coefficients at the first interface. Recall that

$$\eta=\sqrt{\frac{\mu}{\varepsilon}}=\sqrt{\frac{\mu_{\mathrm{r}}\mu_0}{\varepsilon_{\mathrm{r}}\varepsilon_0}}=\frac{\sqrt{\mu_0/\varepsilon_0}}{\sqrt{\varepsilon_{\mathrm{r}}}}=\frac{\eta_0}{n}, \tag{A3}$$

where $\mu_{\mathrm{r}}=1$ is the relative permeability and $n=\sqrt{\varepsilon_{\mathrm{r}}\mu_{\mathrm{r}}}=\sqrt{\varepsilon_{\mathrm{r}}}$ is the refractive index. Thus, we obtain

$$\rho_1=\frac{n_1-n_2}{n_1+n_2}, \tag{A4}$$

$$\tau_1=\frac{2n_1}{n_1+n_2}. \tag{A5}$$

Similarly, the reflection and transmission coefficients at the second interface are obtained as

$$\rho_2=\frac{n_2-n_3}{n_2+n_3}, \tag{A6}$$

$$\tau_2=\frac{2n_2}{n_2+n_3}. \tag{A7}$$

Using the transfer matrix method, we arrive at

$$\begin{aligned} \begin{bmatrix} E_{1+}\\ E_{1-}\end{bmatrix}&=\frac{1}{\tau_1}\begin{bmatrix} 1 & \rho_1\\ \rho_1 & 1\end{bmatrix}\begin{bmatrix} E'_{1+}\\ E'_{1-}\end{bmatrix}\\ &=\frac{1}{\tau_1}\begin{bmatrix} 1 & \rho_1\\ \rho_1 & 1\end{bmatrix}\begin{bmatrix} \mathrm{e}^{\mathrm{i}k_2h} & 0\\ 0 & \mathrm{e}^{-\mathrm{i}k_2h}\end{bmatrix}\begin{bmatrix} E_{2+}\\ E_{2-}\end{bmatrix}\\ &=\frac{1}{\tau_1}\begin{bmatrix} 1 & \rho_1\\ \rho_1 & 1\end{bmatrix}\begin{bmatrix} \mathrm{e}^{\mathrm{i}k_2h} & 0\\ 0 & \mathrm{e}^{-\mathrm{i}k_2h}\end{bmatrix}\frac{1}{\tau_2}\begin{bmatrix} 1 & \rho_2\\ \rho_2 & 1\end{bmatrix}\begin{bmatrix} E'_{2+}\\ 0\end{bmatrix}, \end{aligned} \tag{A8}$$

which can be rewritten as

$$E_{1+}=\frac{\mathrm{e}^{\mathrm{i}k_2h}}{\tau_1\tau_2}\left(1+\rho_1\rho_2\mathrm{e}^{-2\mathrm{i}k_2h}\right)E'_{2+}, \tag{A9}$$

$$E_{1-}=\frac{\mathrm{e}^{\mathrm{i}k_2h}}{\tau_1\tau_2}\left(\rho_1+\rho_2\mathrm{e}^{-2\mathrm{i}k_2h}\right)E'_{2+}. \tag{A10}$$

Once E_{1+} is ascertained, we can calculate E_{1-} and E'_{2+}. Upon inserting these variables into Eq. (A2), the electromagnetic field inside the soft material is known. For simplicity, assume the medium surrounding the left side of the soft material is the same as that surrounding its right side. It follows that

$$n_1=n_3=n^{\mathrm{out}},\quad n_2=n, \tag{A11}$$

$$k_1=k_2=k^{\mathrm{out}},\quad k_2=k. \tag{A12}$$

Incorporating these equations to Eqs. (A4)–(A7), we have

$$\rho_1=-\rho_2=\frac{n^{\mathrm{out}}-n}{n^{\mathrm{out}}+n}=\rho, \tag{A13}$$

$$\tau_1=\frac{2n^{\mathrm{out}}}{n^{\mathrm{out}}+n},\quad \tau_2=\frac{2n}{n^{\mathrm{out}}+n.} \tag{A14}$$

Consider the case when two counter-propagating electromagnetic waves with the same amplitude, frequency, and phase position normally impinge on the soft material sheet (Fig. 2). The corresponding electromagnetic fields can be expressed as

$$\begin{aligned} E_{\mathrm{in}}=&\frac{2\left(1+\rho\right)\cos\left(kz\right)}{\left(1-\rho^2\mathrm{e}^{2\mathrm{i}kh}\right)}\\ &\times E_0\left[\mathrm{e}^{-\mathrm{i}(k^{\mathrm{out}}-k)h/2}-\rho\mathrm{e}^{2\mathrm{i}kh}\mathrm{e}^{-\mathrm{i}(k^{\mathrm{out}}+k)h/2}\right], \end{aligned} \tag{A15}$$

$$\begin{aligned} H_{\mathrm{in}}=&\sqrt{\frac{\varepsilon}{\mu}}\frac{-2\mathrm{i}\left(1+\rho\right)\sin\left(kz\right)}{\left(1-\rho^2\mathrm{e}^{2\mathrm{i}kh}\right)}\\ &\times E_0\left[\mathrm{e}^{-\mathrm{i}(k^{\mathrm{out}}-k)h/2}-\rho\mathrm{e}^{2\mathrm{i}kh}\mathrm{e}^{-\mathrm{i}(k^{\mathrm{out}}+k)h/2}\right], \end{aligned} \tag{A16}$$

$$E_{\mathrm{right}}=E_0\mathrm{e}^{\mathrm{i}k^{\mathrm{out}}z}+\frac{\left(\rho+\mathrm{e}^{\mathrm{i}kh}\right)\left(1-\rho\mathrm{e}^{\mathrm{i}kh}\right)}{\left(1-\rho^2\mathrm{e}^{2\mathrm{i}kh}\right)}E_0\mathrm{e}^{-\mathrm{i}k^{\mathrm{out}}(z+h)}, \tag{A17}$$

$$\begin{aligned} H_{\mathrm{right}}=&\sqrt{\frac{\varepsilon^{\mathrm{out}}}{\mu}}\left[E_0\mathrm{e}^{\mathrm{i}k^{\mathrm{out}}z}\right.\\ &\left.+\frac{\left(\rho+\mathrm{e}^{\mathrm{i}kh}\right)\left(1-\rho\mathrm{e}^{\mathrm{i}kh}\right)}{\left(1-\rho^2\mathrm{e}^{2\mathrm{i}kh}\right)}E_0\mathrm{e}^{-\mathrm{i}k^{\mathrm{out}}(z+h)}\right]. \end{aligned} \tag{A18}$$

Inserting the electromagnetic fields into Eq. (2), we obtain the Maxwell stresses as

$$\langle T_1\rangle_{\mathrm{in}}=\varepsilon E_0^2\frac{(1+\rho)^2\left[1+\rho^2-2\rho\cos\left(kh\right)\right]}{1+\rho^4-2\rho^2\cos\left(2kh\right)}\cos\left(2kz\right), \tag{A19}$$

$$\begin{aligned} \langle T_2\rangle_{\mathrm{in}}=&-\varepsilon E_0^2\frac{(1+\rho)^2\left[1+\rho^2-2\rho\cos\left(kh\right)\right]}{1+\rho^4-2\rho^2\cos\left(2kh\right)}\\ &\times\cos\left(2kz\right), \end{aligned} \tag{A20}$$

$$\langle T_3\rangle_{\mathrm{in}}=-\varepsilon E_0^2\frac{(1+\rho)^2\left[1+\rho^2-2\rho\cos\left(kh\right)\right]}{1+\rho^4-2\rho^2\cos\left(2kh\right)}, \tag{A21}$$

$$\langle T_1 \rangle_{\text{right}} = \varepsilon^{\text{out}} E_0^2 \times \text{Re}\left[\frac{\left(\rho + \mathrm{e}^{\mathrm{i}kh}\right)\left(1 - \rho \mathrm{e}^{\mathrm{i}kh}\right)}{\left(1 - \rho^2 \mathrm{e}^{2\mathrm{i}kh}\right)} \mathrm{e}^{-\mathrm{i}k^{\text{out}}(h+2z)}\right], \tag{A22}$$

$$\langle T_2 \rangle_{\text{right}} = -\varepsilon^{\text{out}} E_0^2 \times \text{Re}\left[\frac{\left(\rho + \mathrm{e}^{\mathrm{i}kh}\right)\left(1 - \rho \mathrm{e}^{\mathrm{i}kh}\right)}{\left(1 - \rho^2 \mathrm{e}^{2\mathrm{i}kh}\right)} \mathrm{e}^{-\mathrm{i}k^{\text{out}}(h+2z)}\right], \tag{A23}$$

$$\langle T_3 \rangle_{\text{right}} = -\varepsilon^{\text{out}} E_0^2. \tag{A24}$$

These Maxwell stresses can be further homogenized as

$$\begin{aligned} t_1 &= -\frac{1}{h}\int_{-h/2}^{h/2} \langle T_1(z) \rangle \mathrm{d}z, \\ t_2 &= -\frac{1}{h}\int_{-h/2}^{h/2} \langle T_2(z) \rangle \mathrm{d}z, \\ t_3 &= \left\langle T_3^{\text{out}}(h) \right\rangle - \langle T_3(h) \rangle . \end{aligned} \tag{A25}$$

Once the electromagnetic fields are known, the Maxwell stresses can be calculated by inserting the electromagnetic fields into Eq. (2) while the equivalent Maxwell stresses are obtained via the homogenization of Eq. (A25). Eventually, the optomechanical response of the soft metamaterial sheet can be analyzed by using Eq. (9) in conjunction with the corresponding mechanical boundary conditions.

References

1. Lee, J.H., Singer, J.P., Thomas, E.L.: Micro-/nanostructured mechanical metamaterials. Adv. Mater. **24**, 4782–4810 (2012)
2. Smith, D.R., Padilla, W.J., Vier, D.C., et al.: Composite medium with simultaneously negative permeability and permittivity. Phys. Rev. Lett. **84**, 4184–4187 (2000)
3. Pendry, J.B.: Negative refraction makes a perfect lens. Phys. Rev. Lett. **85**, 3966–3969 (2000)
4. Schurig, D., Mock, J.J., Justice, B.J., et al.: Metamaterial electromagnetic cloak at microwave frequencies. Science **314**, 977–980 (2006)
5. Nicolaou, Z.G., Motter, A.E.: Mechanical metamaterials with negative compressibility transitions. Nat. Mater. **11**, 608–613 (2012)
6. Lakes, R.S., Lee, T., Bersie, A., et al.: Extreme damping in composite materials with negative-stiffness inclusions. Nature **410**, 565–567 (2001)
7. Moore, B., Jaglinski, T., Stone, D.S., et al.: Negative incremental bulk modulus in foams. Philos. Mag. Lett. **86**, 651–659 (2006)
8. Janmey, P.A., Mccormick, M.E., Rammensee, S., et al.: Negative normal stress in semiflexible biopolymer gels. Nat. Mater. **6**, 48–51 (2007)
9. Lakes, R.: Foam structures with a negative Poisson's ratio. Science **235**, 1038–1040 (1987)
10. Bertoldi, K., Reis, P., Willshaw, S., et al.: Novel negative Poisson's ratio behavior induced by an elastic instability. Adv. Mater. **22**, 361–366 (2010)
11. Baughman, R.H., Shacklette, J.M., Zakhidov, A.A., et al.: Negative Poisson's ratios as a common feature of cubic metals. Nature **392**, 362–365 (1998)
12. Carneiro, V.H., Puga, H., Meireles, J.: Analysis of the geometrical dependence of auxetic behavior in reentrant structures by finite elements. Acta Mech. Sin. **32**, 1–6 (2016)
13. Li, J., Shim, J., Deng, J., et al.: Switching periodic membranes via pattern transformation and shape memory effect. Soft Matter **8**, 10322–10328 (2012)
14. Overvelde, J.T., Kloek, T., D'Haen, J.J., et al.: Amplifying the response of soft actuators by harnessing snap-through instabilities. Proc. Natl. Acad. Sci. U. S. A. **112**, 10863–10868 (2015)
15. Singamaneni, S., Bertoldi, K., Chang, S., et al.: Bifurcated Mechanical Behavior of Deformed Periodic Porous Solids. Adv. Funct. Mater. **19**, 1426–1436 (2009)
16. Shan, S., Kang, S.H., Raney, J.R., et al.: Multistable Architected Materials for Trapping Elastic Strain Energy. Adv. Mater. **27**, 4296–4301 (2015)
17. Xin, F.X., Lu, T.J.: Acoustomechanical constitutive theory for soft materials. Acta Mech. Sin. **32**, 828–840 (2016)
18. Xin, F.X., Lu, T.J.: Tensional acoustomechanical soft metamaterials. Sci. Rep. **6**, 27432 (2016)
19. Ploschner, M., Mazilu, M., Krauss, T.F., et al.: Optical forces near a nanoantenna. J. Nanophotonics **4**, 471–478 (2010)
20. Maclure, M.: Radiation pressure and the linear momentum of the electromagnetic field. Opt. Express **12**, 5375–5401 (2004)
21. Cui, J., Björnmalm, M., Liang, K., et al.: Super-soft hydrogel particles with tunable elasticity in a microfluidic blood capillary model. Adv. Mater. **26**, 7295–7299 (2014)
22. Chakrabarti, A., Chaudhury, M.K.: Direct measurement of the surface tension of a soft elastic hydrogel: exploration of elastocapillary instability in adhesion. Langmuir **29**, 6926–6935 (2013)
23. Ashkin, A., Dziedzic, J.M., Bjorkholm, J.E., et al.: Observation of a single-beam gradient force optical trap for dielectric particles. Opt. Lett. **11**, 288–290 (1986)
24. Chu, S.: Laser manipulation of atoms and particles. Science **253**, 861–866 (1991)
25. Dienerowitz, M., Mazilu, M., Dholakia, K.: Optical manipulation of nanoparticles: a review. J. Nanophotonics **2**, 269–270 (2008)
26. Jonás, A., Zemánek, P.: Light at work: the use of optical forces for particle manipulation, sorting, and analysis. Electrophoresis **29**, 4813–4851 (2008)
27. Dao, M., Lim, C.T., Suresh, S.: Mechanics of the human red blood cell deformed by optical tweezers. J. Mech. Phys. Solids **51**, 2259–2280 (2003)
28. Guck, J., Ananthakrishnan, R., Moon, T.J., et al.: Optical deformability of soft biological dielectrics. Phys. Rev. Lett. **84**, 5451–5454 (2000)
29. Casner, A., Delville, J.P.: Giant deformations of a liquid-liquid interface induced by the optical radiation pressure. Phys. Rev. Lett. **87**, 603–604 (2001)
30. Casner, A., Delville, J.P.: Laser-induced hydrodynamic instability of fluid interfaces. Phys. Rev. Lett. **90**, 144503 (2003)
31. Schroll, R.D., Wunenburger, R., Casner, A., et al.: Liquid transport due to light scattering. Phys. Rev. Lett. **98**, 133601 (2006)
32. Li, M., Pernice, W.H., Xiong, C., et al.: Harnessing optical forces in integrated photonic circuits. Nature **456**, 480–484 (2008)
33. Pernice, W.H.P., Li, M., Tang, H.X.: Theoretical investigation of the transverse optical force between a silicon nanowire waveguide and a substrate. Opt. Express **17**, 1806–1816 (2009)
34. Povinelli, M.L., Ibanescu, M., Johnson, S.G., et al.: Slow-light enhancement of radiation pressure in an omnidirectional-reflector waveguide. Appl. Phys. Lett. **85**, 1466–1468 (2004)
35. Povinelli, M.L., Loncar, M., Ibanescu, M., et al.: Evanescent-wave bonding between optical waveguides. Opt. Lett. **30**, 3042–3044 (2005)
36. Ren, M., Huang, J., Cai, H., et al.: Nano-optomechanical actuator and pull-back instability. Acs Nano **7**, 1676–1681 (2013)

37. Thourhout, D.V., Roels, J.: Optomechanical device actuation through the optical gradient force. Nat. Photonics **4**, 211–217 (2010)
38. Juodkazis, S., Mukai, N., Wakaki, R., et al.: Reversible phase transitions in polymer gels induced by radiation forces. Nature **408**, 178–181 (2000)
39. Gent, A.N.: A New Constitutive Relation for Rubber. Rubber Chem. Technol. **69**, 59–61 (2012)
40. Bai, R., Suo, Z.: Optomechanics of Soft Materials. J. Appl. Mech. **82**, 071011 (2015)